A WAVEFIELD-BASED EARTHQUAKE EARLY WARNING ALGORITHM IN THE JAPANESE NATIONWIDE SYSTEM AND IMPROVEMENT PLANS

Y. Kodera[(1)]

[(1)] *Researcher, Meteorological Research Institute, Japan Meteorological Agency, y_kodera@mri-jma.go.jp*

Abstract

An important factor that determines the reliability of earthquake early warning (EEW) systems is the robustness of ground motion prediction for complex earthquake scenarios. Many EEW systems that have been developed or are operational use point-source model algorithms in which an earthquake location is estimated using the initial P-wave arrivals with the assumption of negligible source finiteness. The point-source approach, however, is likely to fail to provide accurate and timely ground motion predictions for earthquakes with large finite faults and multiple simultaneous events. To enhance the system robustness, the Japan Meteorological Agency (JMA) introduced the Propagation of Local Undamped Motion (PLUM) method (Kodera et al., 2018) into its nationwide EEW system in March 2018. PLUM is a wavefield-based approach that predicts ground shaking directly from ongoing observed seismic intensity distribution, without source parameter estimation. PLUM predicts seismic intensities assuming that ongoing ground motion will propagate without attenuation if the propagation distance is as short as ≤30 km. Kodera et al. (2018) showed that PLUM provided accurate ground motion predictions for the 2011 M_w 9.0 Tohoku-Oki earthquake, for which a point-source algorithm underpredicted the strong motion due to magnitude saturation and nonnegligible fault finiteness.

On the other hand, PLUM has a shortcoming in terms of timeliness. Long lead times are not expected because PLUM only uses observed intensities within 30 km from target sites so that accurate intensity predictions are not provided until the strong motion reaches at a close distance. The theoretical maximum time is 10 s, with the assumption that the S-wave velocity is 3 km/s. To enhance the PLUM timeliness, we improved the prediction procedure focusing on (1) the use of P-waves and (2) distance attenuation models.

For the P-wave incorporation, we introduce an on-site algorithm that detects P-wave arrivals and predicts S-wave intensity from the corresponding P-wave intensity. An on-site ground motion prediction is input to the PLUM calculation instead of an intensity observation if the on-site prediction is available. When this approach was applied to the Tohoku-Oki earthquake using KiK-net stations, lead times were lengthened by several seconds for sites close to the source region without largely decreasing the prediction accuracy. This result suggests that the P-wave incorporation enables PLUM to shorten the required time to issue the first warning.

For the incorporation of distance attenuation models, we used ground motion prediction equations (GMPEs). A distance attenuation relationship between an observation station and a target site was estimated by monitoring the surrounding intensity distribution around the observation station and fitting a GMPE function with the surrounding intensities. The predicted intensity at the target site was then calculated using the best-fit function. When the proposed method was applied to the Tohoku-Oki earthquake using KiK-net and K-NET stations, available lead times were ~10 s longer for sites with low intensities (i.e., distant sites from the source region). This finding indicates that the incorporation of distance attenuation models contributes to issuing the first warning for a wider area.

Keywords: earthquake early warning; P-wave; ground motion prediction equation; PLUM algorithm; on-site ground motion prediction

1. Introduction

Earthquake early earning (EEW) systems, which analyze observed seismic signals in real time and warn of impending strong shaking before the actual ground motion hits, have been developed and implemented in many earthquake-prone regions to minimize earthquake damage (e.g., [1]). In Japan, the Japan Meteorological Agency (JMA) has been operating its nationwide EEW system since October 2007 [2]. At the beginning, the system was based solely on point-source algorithms. The algorithms first estimated source parameter (location and magnitude) from P-wave arrivals and displacement amplitudes assuming negligible fault finiteness and then calculated ground motion predictions using a 1-dimensional ground motion prediction equation (GMPE) proposed by Si and Midorikawa (1999) [3–5]. The system exhibited high performance until 2010; however, the occurrence of the 2011 M_w9.0 earthquake highlighted technical limitations of the point source approach (e.g., [6]). First, the point source approximation underpredicted the ground motions of the M_w9.0 earthquake in the area to the south west of the source region, near the earthquake's fault but far from the initial rupture point. For the subsequent aftershock sequence, the system overpredicted seismic intensities because of incorrect association of P-wave arrivals and resulting mislocation of estimated sources. Also, the system missed several large earthquakes just after the mainshock. Their P-wave arrivals were not detected by the STA/LTA (the ratio of short- to long-time averages) algorithm (e.g., [7]) because waveforms of multiple events were overlapped with each other.

To address those technical challenges, JMA introduced the propagation of local undamped motion (PLUM) algorithm, a simple wavefield-based ground motion prediction algorithm [8], into the EEW system in March 2018. PLUM predicts ground motions directly from actual observations, without source parameter estimation. PLUM calculates $Ir_{\mathrm{pred}}^{(i\to x)}$, a predicted seismic intensity at a target site located at position x from an observation station at position i, by

$$Ir_{\mathrm{pred}}^{(i\to x)} = Ir_{\mathrm{obs}}^{(i)} - F_{Ir}^{(i)} + F_{Ir}^{(x)}, \tag{1}$$

where $Ir_{\mathrm{obs}}^{(i)}$ is an intensity at the observation station, and $F_{Ir}^{(i)}$ and $F_{Ir}^{(x)}$ are site factors at i and x, respectively (intensity differences from a reference site on bedrock). Then, a predicted intensity $Ir_{\mathrm{pred}}^{(x)}$ is given by

$$Ir_{\mathrm{pred}}^{(x)} = \max_{i \in C_R} Ir_{\mathrm{pred}}^{(i\to x)}, \tag{2}$$

where C_R indicates a circular region centered at x with a radius of R. R is usually set to 30 km. These equations assume that future wave propagation can be approximated as superposition of unattenuated plane waves propagating within a distance as short as R from each observation point. PLUM provides ground motion predictions independently of earthquake occurrences and requires no assumption of specific source models; therefore, PLUM could exhibit high robustness for complex earthquake scenarios such as large earthquakes with nonnegligible finite fault ruptures and intense seismic activities within a short time and distance. A retrospective simulation using the Tohoku-Oki earthquake and subsequent aftershocks showed that PLUM predicted ground motions for the mainshock and aftershock activity with higher accuracy and processed large events just after the mainshock with a higher detection rate than the point-source algorithms [8]. A recent study analyzing the first-year PLUM performance in the operational JMA EEW system indicated that PLUM contributed to the improvement of timely public warning issuance for damaging inland earthquakes [9].

Althogh PLUM could provide accurate ground motion predictions with high robustness, the algorithm has a weak point in that available lead times are limited to ≤10 s in theory, assuming $R = 30$ km and V_S (S-wave velocity) = 3 km/s. High intensities are not predicted until the correspnding strong motions have propagated at a close distance from a target site. Main reasons for the limited lead times are (1) that ground motion predictions are based mainly on S-wave observations and do not use P-wave information and (2) that the prediction radius R can not be lengthened because of the assumption of uunattenuated wave propagtion. In this study, we develop new prediction procedures considering P-waves and distance attenuation relations to improve the PLUM timeliness.

In this article, all site factors are assumed to be adjusted to KiK-net borehole sensor IBRH19 using the method proposed by Ogiso et al. (2016) [10].

2. Incorporation of P-waves into PLUM

To enhance the PLUM timeliness, we first focus on incorporating P-waves into PLUM. A ground motion prediction can be made just after P-wave arrivals, without waiting for S-waves, if the S-wave intensities can be estimated from the corresponding P-wave observations. We therefore developed an on-site prediction algorithm from P- to S-wave intensities [11].

2.1. On-site prediction algorithm

Our on-site algorithm is divided into two parts: real-time P-wave detection and S-wave intensity prediction.

In the P-wave detection part, P-waves are identified based on the principal component analysis for particle motions. The particle motions are obtained from accelerations (band-pass filtered at 0.5–10 Hz) with a 4-s time window sliding every 0.1 s. P-filter value p is then calculated using eigen values λ_i ($i = 1, 2, 3;\ \lambda_1 \geq \lambda_2 \geq \lambda_3$) and vectors u_{ij} [12]:

$$p = r\cos\theta, \tag{3}$$

$$r = 1 - \frac{\lambda_2 + \lambda_3}{2\lambda_1}, \tag{4}$$

$$\cos\theta = u_{13}, \tag{5}$$

where r and $\cos\theta$ are the rectilinearity and vertical incident angle of the particle motion. The algorithm classfies the waveform as a P-wave if p exceeds a certain threshold p_{th} (p_{th} is set to 0.4 in this study).

After the P-wave detection, S-wave on-site predictions are made. If $p \geq p_{\mathrm{th}}$, a predicted S-wave intensity Ir_{os} is given by

$$Ir_{\mathrm{os}} = Ir_{\mathrm{obs}}[\mathrm{UD}] + \Delta Ir_{PS}, \tag{6}$$

where $Ir_{\mathrm{obs}}[\mathrm{UD}]$ is an observed intensity calculated only from the UD component (the original intensity measurement is defined using the vector sum of the three components), an approximation to the detected P-wave intensity, and ΔIr_{PS} is an intensity difference between P- and S-waves, set to 1.0 in this study based on an empirical relation mentioned in Yamamoto et al. 2008 [13].

A distinctive feature of the proposed approach is continuous P-wave detection for the entire earthquake waveform. Many previous studies using P-waves to predict ground motions focused only on the time window from the initial P-wave onset to the initial S-wave arrival (e.g., [4] and [14–16]); however, the algorithm conducts the P-wave detection and S-wave intensity prediction even after the S-wave onset. As mentioned later, this continuous detection approach allows the system to recognize late onset P-waves from growing ruptures.

2.2. Application to the M_w9.0 Tohoku-Oki earthquake

We applied the on-site prediction algorithm to the M_w9.0 Tohoku-Oki earthquake using KiK-net borehole stations.

Figure 1a showed on-site prediction results for station MYGH04. High P-filter values appeared not only the P-wave time window of the initial rupture point but also those of the first and second strong motion generation areas (SMGAs; each SMGA is defined based on Asano and Iwata (2012) [17]), indicating that the algorithm detected P-waves from the SMGAs in addition to that from the initial rupture point. S-wave intensity predictions were made for the SMGAs, and those peaks were predicted with high accuracy. Those results suggested that the algorithm could exhibit high performance for a complex, long-lasting rupture of a large earthquake.

We also calculated PLUM predictions incorporating the on-site algorithm (Fig. 1b). For the new PLUM prediction algorithm, Ir_{os} is used instead of an intensity observation if Ir_{os} is available. When applied to the

Tohoku-Oki event, the modified PLUM algorithm predicted intensities with the same accuracy as the original PLUM algorithm for target sites with high intensity observations (i.e., sites very close to the source region). For those sites, the modified algorithm provided several to ten seconds longer lead times than the original, indicating that the proposed algorithm enhanced the timeliness for sites that have the the high potential to experience severe earthquake damage, without facing the trade-off relationship between prediction accuracy and timeliness. On the other hand, the modified algorithm overpredicted intensities for sites with relatively low intensity observations. One of the reasons for the overprediction was misdetecting P-waves at coda and surface wave parts; therefore, further studies on the P-wave detection would be required in the future to improve the algorithm performance.

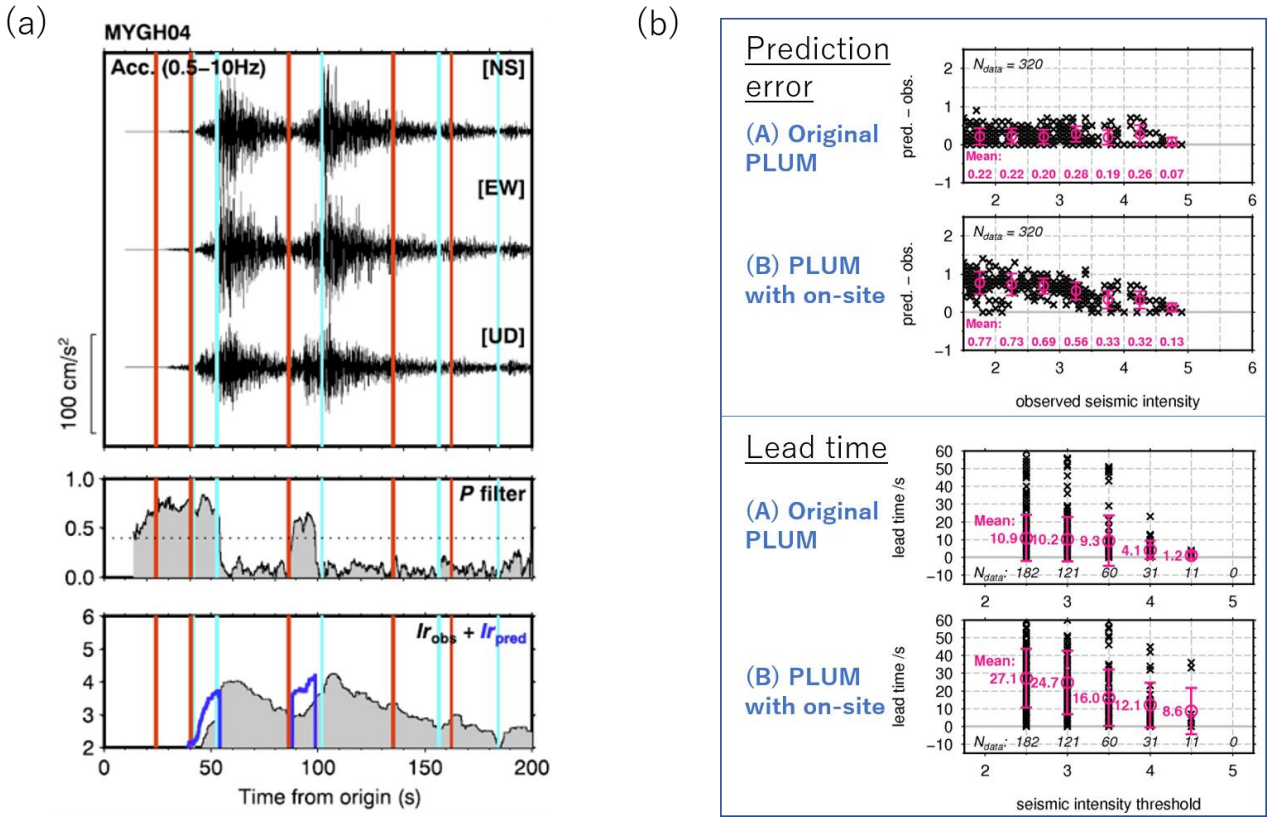

Figure 1. (a) An example of the P-wave detection and S-wave intensity prediction by the proposed on-site algorithm for KiK-net borehole station MYGH04 during the M_w 9.0 Tohoku-Oki earthquake. Three-component accelerations (top panel), P-filter values (middle), and observed (gray) and predicted (blue) intensities (bottom) are shown. Vertical lines indicate the theoretical P- (vertical red lines) and S-wave (cyan) onsets of the initial rupture point and four SMGAs [17]. (b) Prediction errors and lead times provided by the original and modified PLUM algorithms for individual target sites during the Tohoku-Oki event. Magenta symbols indicate means and standard deviations with the exact number of the mean values. The prediction errors were obtained by the intensity differences between the peak prediction and observation. Lead times were computed from the time differences between when the prediction and observation exceeded a given intensity threshold.

3. Incorporation of distance attenuation into PLUM

Second, we tried to incorporate distance attenuation relations into PLUM and lengthen the prediction radius R from 30 km without overprediction.

3.1. Real-time estimation of distance attenuation relations

Our proposed algorithm estimates localized distance attenuation relations for each observation station ([18]; Fig. 2). A distance attenuation relation around a certain observation station (hereafter referred to as the reference observation station) is evaluated by monitoring real-time observations at surrounding observation stations (stations located within R_{obs} from the reference station; Fig. 2a). An assumed distance attenuation model f is fitted with the actual observed intensities. Then, predicted intensities for target sites within R_{pred} ($>$ 30 km) are calculated by extrapolating the estimated attenuation relation.

A ground motion prediction $Ir_{\mathrm{pred}}^{(i\to x)}$, a predicted intensity for a target site at position x from the reference observation station at position i, is calculated by

$$Ir_{\mathrm{pred}}^{(i\to x)} = f\left(Ir_{\mathrm{obs}}^{(i)}, \Delta_{ix}, Ir_{\mathrm{obs}}^{(k)}, Ir_{\mathrm{obs}}^{(l)}, \cdots\right), \tag{7}$$

where $Ir_{\mathrm{obs}}^{(i)}$ is an observed intensity at the reference station, Δ_{ix} is a distance between positions i and x, and $Ir_{\mathrm{obs}}^{(k)}, Ir_{\mathrm{obs}}^{(l)}, \cdots$ are observed intensities at the surrounding stations. In this study, we employed a distance attenuation function f modeled with a point-source hypocenter just below the reference station and a GMPE function, imitating elementary wave propagation in the Huygens principle:

$$f\left(Ir_{\mathrm{obs}}^{(i)}, \Delta_{ix}, Ir_{\mathrm{obs}}^{(k)}, Ir_{\mathrm{obs}}^{(l)}, \cdots\right) = G\left(\theta^{(i)}, \Delta_{ix}\right), \tag{8}$$

where G is a GMPE function, and $\theta^{(i)} = \{lat, lon, d, M\}$ (hypocentral latitude, longitude, depth, and JMA magnitude, respectively) is a set of parameters of the point-source model (Fig. 2b). In this study, the GMPE function proposed by Si and Midorikawa (1999) [3] was used as G. The depth and magnitude of $\theta^{(i)}$ is estimated from $Ir_{\mathrm{obs}}^{(i)}$ and $Ir_{\mathrm{obs}}^{(k)}, Ir_{\mathrm{obs}}^{(l)}, \cdots$. A set of source parameters $\theta = \theta_1, \cdots, \theta_N$ with different depths $d = d_1, \cdots, d_N$ and $M = M_1, \cdots, M_N$ is assumed (N is the number of assumed sources; each d_n ($n = 1, \cdots, N$) and N are given as predefined fixed parameters). The most appropriate θ is selected as $\theta^{(i)}$ based on the actual observations of $Ir_{\mathrm{obs}}^{(i)}$ and $Ir_{\mathrm{obs}}^{(k)}, Ir_{\mathrm{obs}}^{(l)}, \cdots$, minimizing the root mean square error between the assumed GMPE function and those observed intensities. The residual is evaluated using surrounding stations with the first to K-th lowest observed intensites (K is a given parameter) only, assuming that the wave is propagating to the direction of the maximum gradient of the intensity distribution.

$Ir_{\mathrm{pred}}^{(x)}$, the final output of the predicted intensity for the target site at x, is given by the same equation as equation (2) but using a circular region with a radius of R_{pred}.

Two types of point-source models were employed to model the function f: point-source with/without consideration of fault distance. For the model with the fault-distance consideration, we used $R_{\mathrm{obs}} = 45$ km, $R_{\mathrm{pred}} = 300$ km, $d = 1.00$, 1.46, 2.14, 3.13, 4.58, 6.71, 9.82, 14.36, 21.02, 30.75, and 45.00 km ($N = 11$; these depths are equally divided with logarithmic spacing). For the model without the fault-distance consideration, we used $R_{\mathrm{obs}} = 45$ km, $R_{\mathrm{pred}} = 60$ km, and $d = 1.00$ km ($N = 1$).

3.2. Application to the M_w9.0 Tohoku-Oki earthquake

We evaluated the performance of the proposed algorithm, applying to the Tohoku-Oki earthquake (Fig. 3). KiK-net and K-NET stations were used for the simulation. The proposed algorithm predicted intensities for all sites with accuracy higher than or equivalent to the original PLUM algorithm. For sites with relatively low observed intensities (i.e., sites with the potential to obtain long lead times because of their locations far from the source region), the proposed algorithm provided ~10 s longer lead times than PLUM, focusing on the median values. This indicates that introducing distance attenuation relations allow the system to improve the

timeliness of the first warning issuance for distant areas. For sites with higher intensity observations, lead times given by the proposed algorithm were shorter than those by PLUM. One of the reasons was that the proposed algorithm needed to be waiting until the strong motion had propagated completely with in the R_{obs} region to estimate the accurate distance attenuation relation for observation stations closest to the rupture area, although PLUM computed predicted intensities immediately after the observation stations detected the strong motion. For the actual operation, it might be better to use the original PLUM and proposed algorithms at the same time, taking the maximum of predicted intensities obtained from the both algorithms.

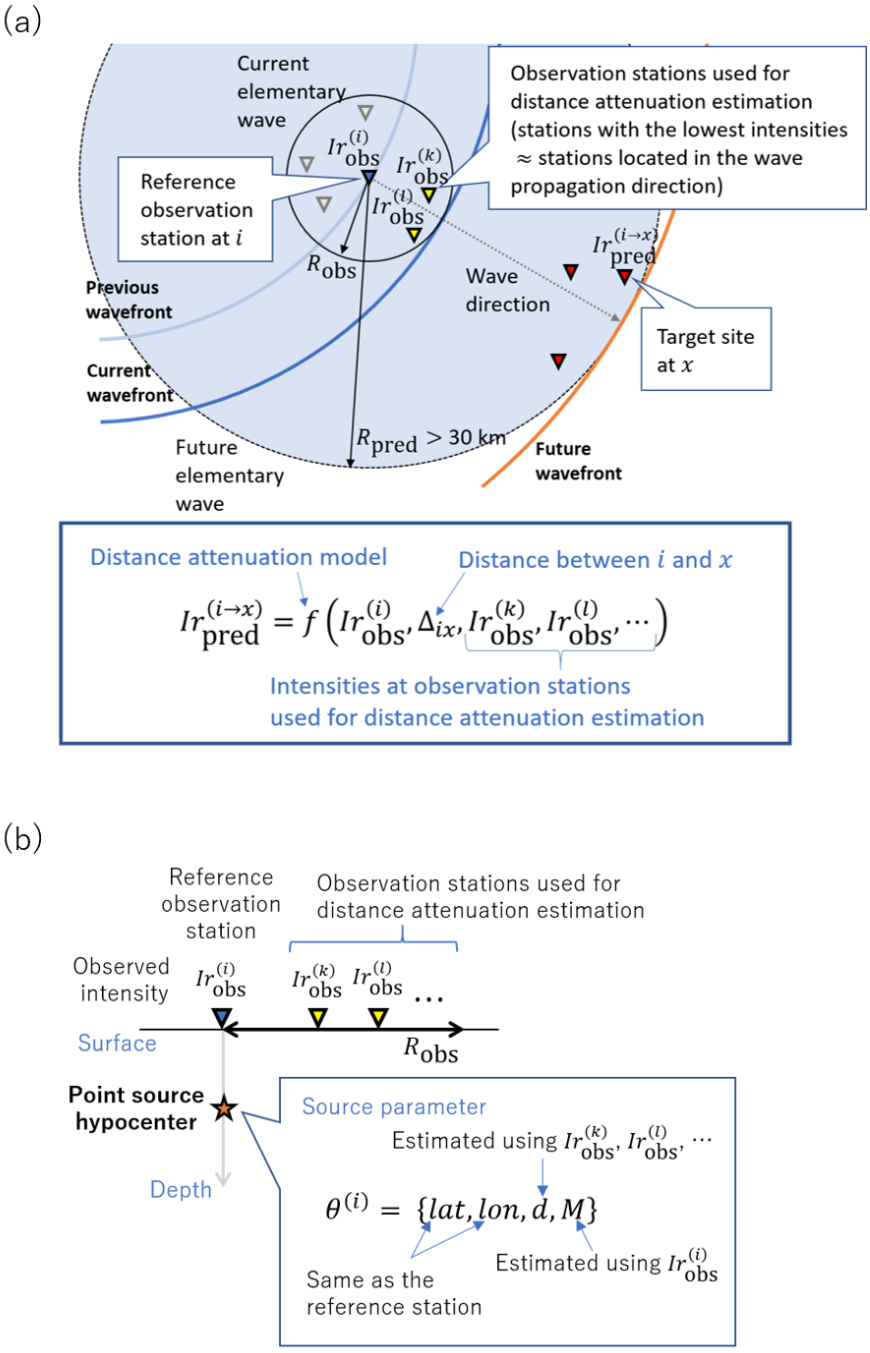

Figure 2. (a) Schematic illustration of the ground motion prediction algorithm with the distance attenuation estimation in real time. (b) Virtual point source to model the distance attenuation function f.

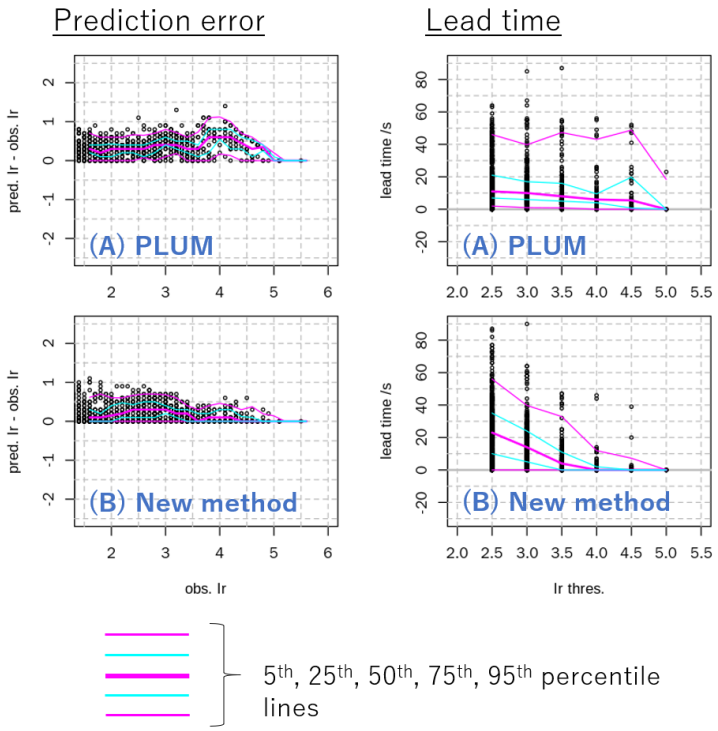

Figure 3. Comparisons of prediction errors and available lead times for the original PLUM algorithm and proposed algorithm incorporating the real-time estimation of distance attenuation relations. The definitions of the prediction errors and lead times are the same as in Fig. 1b.

4. Conclusions

To enhance the PLUM performance in terms of the ground motion prediction timeliness, we developed new algorithms that predict ground motions (1) using an on-site S-wave intensity prediction based on the continuous P-wave detection and (2) using distance attenuation relations estimated by monitoring surrounding observed intensities in real time. The applications of these algorithms to the M_w9.0 Tohoku-Oki earthquake showed (1) that incorporating P-waves could lengthen lead times for sites close to the source region without decreasing the prediction accuracy compared with the original PLUM algorithm and (2) that incorporating distance attenuation relations could enable the system to provide longer lead times for sites with relatively distant from the rupture area (i.e., sites with a potential to obtain long lead times). Therefore, these approaches could be promising candidates for improving the entire performance of EEW systems employing wavefield-based ground motion prediction algorithms.

5. Acknowledgments

We used waveforms recorded at KiK-net and K-NET stations of the National Research Institute for Earth Science and Disaster Resilience [19].

6. References

[1] Allen RM, Melgar D (2019): Earthquake early warning: Advances, scientific challenges, and societal needs. *Annual Review of Earth and Planetary Sciences,* **47**, 361–388.

[2] Hoshiba M, Kamigaichi O, Saito M, Tsukada S, Hamada N (2008): Earthquake early warning starts nationwide in Japan. *Eos, Transactions of the American Geophysical Union,* **89,** 73–74.

[3] Si H, Midorikawa S (1999): New attenuation relationships for peak ground acceleration and velocity considering effects of fault type and site condition. *Journal of Structural and Construction Engineering, AIJ,* **64(523),** 63–70 (in Japanese).

[4] Kamigaichi O (2004): JMA earthquake early warning. *Journal of Japan Association for Earthquake Engineering,* **4(3),** 134–137.

[5] Iwakiri K, Hoshiba M, Nakamura K, Morikawa N (2011): Improvement in the accuracy of expected seismic intensities for earthquake early warning in Japan using empirically estimated site amplification factors. *Earth, Planets and Space,* **63(2),** 57–69.

[6] Hoshiba M, Iwakiri K, Hayashimoto N, Shimoyama T, Hirano K, Yamada Y, Ishigaki Y, Kikuta H (2011): Outline of the 2011 off the Pacific coast of Tohoku earthquake (Mw 9.0)—Earthquake early warning and observed seismic intensity—. *Earth, Planets and Space,* **63,** 547–551.

[7] Allen RV (1978): Automatic earthquake recognition and timing from single traces, *Bulletin of the Seismological Society of America,* **68,** 1521–1532.

[8] Kodera Y, Yamada Y, Hirano K, Tamaribuchi K, Adachi S, Hayashimoto N, Morimoto M, Nakamura M, Hoshiba M (2018): The propagation of local undamped motion (PLUM) method: A simple and robust seismic wavefield estimation approach for earthquake early warning. *Bulletin of the Seismological Society of America,* **108(2),** 983–1003.

[9] Kodera Y, Hayashimoto N, Moriwaki K, Noguchi K, Saito J, Akutagawa J, Adachi S, Morimoto M, Okamoto K, Honda S, Hoshiba M (2020): First-year performance of a nationwide earthquake early warning system using a wavefield-based ground-motion prediction algorithm in Japan, *Seismological Research Letters* (in press).

[10] Ogiso M, Aoki S, Hoshiba M (2016): Real-time seismic intensity prediction using frequency-dependent site amplification factors, *Earth, Planets and Space,* **68(1),** 83.

[11] Kodera Y (2018): Real-time detection of rupture development: Earthquake early warning using P waves from growing ruptures. *Geophysical Research Letters,* **45,** 156–165.

[12] Ross ZE, Ben-Zion Y (2014): Automatic picking of direct P, S seismic phases and fault zone head waves. *Geophysical Journal International,* **199(1),** 368–381.

[13] Yamamoto S, Rydelek P, Horiuchi S, Wu C, Nakamura H (2008): On the estimation of seismic intensity in earthquake early warning systems. *Geophysical Research Letters,* **35,** L07302.

[14] Nakamura Y (1988): On the urgent earthquake detection and alarm system (UrEDAS). In Proceedings of Ninth World Conference on Earthquake Engineering, Tokyo and Kyoto, Japan, August 2–9, 1988, **7,** 673–678.

[15] Olson EL, Allen RM (2005): The deterministic nature of earthquake rupture. *Nature,* **438(7065),** 212–215.

[16] Colombelli S, Zollo A, Festa G, Picozzi M (2014): Evidence for a difference in rupture initiation between small and large earthquakes. *Nature Communications,* **5,** 3958.

[17] Asano K, Iwata T (2012): Source model for strong ground motion generation in the frequency range 0.1–10 Hz during the 2011 Tohoku earthquake, *Earth, Planets and Space,* **64,** 1111–1123.

[18] Kodera Y (2019): An earthquake early warning method based on Huygens principle: Robust ground motion prediction using various localized distance-attenuation models, *Journal of Geophysical Research: Solid Earth,* **124,** 12,981–12,996.

[19] National Research Institute for Earth Science and Disaster Resilience (NIED) (2019): NIED K-NET, KiK-net.

